SCIENCE CHINA
Chemistry

• ARTICLES •

January 2012 Vol.55 No.1: 182–194
doi: 10.1007/s11426-011-4370-3

Adsorption of Eu(III) on titanate nanotubes studied by a combination of batch and EXAFS technique

SHENG GuoDong†, YANG ShiTong†, ZHAO DongLin, SHENG Jiang & WANG XiangKe*

Key Laboratory of Novel Thin Film Solar Cells; Institute of Plasma Physics, Chinese Academy of Sciences, Hefei 230031, China

Received May 4, 2011; accepted July 4, 2011; published online August 31, 2011

The effects of pH, contact time and natural organic ligands on radionuclide Eu(III) adsorption and mechanism on titanate nanotubes (TNTs) are studied by a combination of batch and extended X-ray absorption fine structure (EXAFS) techniques. Macroscopic measurements show that the adsorption is ionic strength dependent at pH < 6.0, but ionic strength independent at pH > 6.0. The presence of humic acid (HA) / fulvic acid (FA) increases Eu(III) adsorption on TNTs at low pH, but reduces Eu(III) adsorption at high pH. The results of EXAFS analysis indicate that Eu(III) adsorption on TNTs is dominated by outer-sphere surface complexation at pH < 6.0, whereas by inner-sphere surface complexation at pH > 6.0. At pH < 6.0, Eu(III) consists of ~ 9 O atoms at $R_{Eu-O} \approx 2.40$ Å in the first coordination sphere, and a decrease in N_{Eu-O} with increasing pH indicates the introduction of more asymmetry in the first sphere of adsorbed Eu(III). At long contact time or high pH values, the Eu(III) consists of ~2 Eu at $R_{Eu-Eu} \approx 3.60$ Å and ~ 1 Ti at $R_{Eu-Ti} \approx 4.40$ Å, indicating the formation of inner-sphere surface complexation, surface precipitation or surface polymers. Surface adsorbed HA/FA on TNTs modifies the species of adsorbed Eu(III) as well as the local atomic structures of adsorbed Eu(III) on HA/FA−TNT hybrids. Adsorbed Eu(III) on HA/FA–TNT hybrids forms both ligand-bridging ternary surface complexes (Eu-HA/FA–TNTs) as well as surface complexes in which Eu(III) remains directly bound to TNT surface hydroxyl groups (i.e., binary Eu–TNTs or Eu-bridging ternary surface complexes (HA/FA–Eu–TNTs)). The findings in this work are important to describe Eu(III) interaction with nanomaterials at molecular level and will help to improve the understanding of Eu(III) physicochemical behavior in the natural environment.

titanate nanotubes, radionuclide Eu(III), extended X-ray absorption fine structure (EXAFS) spectroscopy, humic acid, fulvic acid

1 Introduction

Since the innovative work of Kasuga *et al*. [1, 2], titanate nanotubes (TNTs) have come under intense multidisciplinary studies as sensors, catalyst supports, ion-exchange materials and superior adsorbents due to their fascinating microstructures and excellent physicochemical properties [3]. In the past few years, various investigations have been conducted to study the interaction behavior of TNTs towards organic dyes [4–6] and heavy metal ions [7–9], and it was generally observed that the TNTs were efficient adsorbents for the removal of environmental pollutants in water. However, these limited studies only focused on the adsorption kinetics and thermodynamic properties of TNTs towards organic dyes and heavy metals by batch technique at the macroscopic level and no attention has been paid to radionuclide adsorption onto TNTs, especially the investigation of species and local atomic structures of radionuclide at the molecular level. Furthermore, as the costs of commercially available TNTs are continuously decreasing, it is possible to use these novel nanomaterials, regardless of their high unit cost at the present time, for environmental pollutants removal in wastewater treatment in near future.

In the context of the assessment of radionuclide mobility, knowledge of interaction mechanism is of great importance

*Corresponding author (email: xkwang@ipp.ac.cn)
†Contributed equally to this work.

to assess the radionuclide behavior [10, 11]. In this context, interaction of Eu(III), a chemical analogue of trivalent lanthanides and actinides, with various mineral phases was extensively studied by using batch and spectroscopic techniques [10–14]. Many mechanisms have been postulated for Eu(III) interaction with minerals, including ion exchange, outer-sphere and inner-sphere surface complexation and incorporation into particle lattice [10–12]. In the past decades, EXAFS technique is increasingly used to differentiate the adsorption species and local atomic structures of metal ions [10–15].

Humic substances (HSs), such as humic acid (HA) and fulvic acid (FA), have attracted great attention because of their high complexation ability with radionuclides [10, 11]. For the assessment of radionuclide mobility, the interaction between radionuclides and HSs has been the subject of various studies [10–12, 14]. The study on the influence of HSs and related low molecular weight organic acids (e.g., EDTA, citrate, glutamate) on metal ion adsorption at solid-water interfaces indicated that the functional groups of HSs formed strong complexes with both metal ions and solid surfaces [10–12]. Generally, the adsorption of metal ions is enhanced at low pH, and is reduced at high pH. However, according to our literature survey, no available studies have been performed to identify the influence of HSs on metal ion adsorption onto TNTs, especially at the molecular level.

To better understand the interaction of TNTs with Eu(III), batch experiments are applied to evaluate the effects of reaction time, pH and HA/FA on Eu(III) adsorption to TNTs. Additional information about interatomic distances and coordination numbers of the adsorbed Eu(III) is derived from Eu(III) L_{III}-edge EXAFS spectroscopy analysis. The main purpose of the paper is to study the interaction of Eu(III) with TNTs by a combination of batch and spectroscopy methods, and to understand the mechanism at a molecular level.

2 Experimental section

2.1 Materials and chemicals

All the chemicals studied in the experiments were purchased in analytical purity and used without any further purification. Milli-Q water was used in the experiments. Eu(III) stock solution was prepared from Eu_2O_3 after dissolution, evaporation and redissolution in 10^{-3} mol/L $HClO_4$.

TNTs were prepared using a hydrothermal process with TiO_2 (P25), which is similar to that described by Kasuga *et al*. [1, 2]. The TiO_2 source used for the preparation of TNTs was P25 (Degussa AG, Germany), with a crystalline structure of ca. 20% rutile and ca. 80% anatase and a primary particle size of ca. 30 nm. In a typical preparation, 3 g of the TiO_2 powder was mixed with 90 mL of 10 mol/L NaOH solution followed by hydrothermal treatment of the mixture at 150 °C in a 250-mL teflon-lined autoclave for 24 h. After hydrothermal reaction, the precipitate was separated by filtration and washed with 0.1 mol/L HCl solution and distilled water until the pH value of the rinsing solution reached ca. 7.0. The derived samples were dried in a vacuum oven at 120 °C for 8 h and stored in the glass bottles.

HA and FA were extracted from the soil of Hua-Jia county (Gansu province, China) and characterized in detail [10, 16, 17]. Cross-polarization magic angle spinning (CPMAS) ^{13}C NMR spectra of HA and FA were divided into four chemical shift regions, i.e., 0–50 ppm, 51–105 ppm, 106–160 ppm, and 161–200 ppm. These regions were referred to as aliphatic, carbohydrate, aromatic, and carboxyl regions. The percentage of total intensity for each region is calculated by integrating the CPMAS ^{13}C NMR spectra with each region, and the fractions of aromatic groups calculated by expressing aromatic C as percentage of the sum of aliphatic C (0–105 ppm) + aromatic C (106–160 ppm) are listed in Table 1. HA and FA have also been characterized as a suite of 3 discrete acids with pK_a values listed in Table 2. The concentrations of functional groups of HA and FA determined by fitting the potentiometric titration data using FITEQL 3.1 are given in Table 2. The weight-averaged molecular weights (M_w) of dissolved HA and FA are determined according to the method of Chin *et al*. [18], and the M_w values of dissolved HA and FA are calculated to be 2108 and 1364, respectively.

2.2 Batch experiments

Batch adsorption experiments were conducted in polyethylene tubes at $T = 20 \pm 1$ °C under N_2 conditions. The aqueous suspension was mixed with a solution containing

Table 1 ^{13}C NMR characteristics (Chemical Shift ppm) of HA and FA [10, 16, 17]

HSs	0–50	51–105	106–160	161–200	Aromaticity
FA	16	28	19	39	30
HA	15	21	47	17	57

Table 2 The concentrations of functional groups of HA and FA calculated from potentiometric acid-base titration by using FITEQL 3.1 [10, 16, 17]

	LogK_a			C (mol/g)*			Surface sites density (mol/g)	WSOS/DF
	L_1	L_2	L_3	HL_1	HL_2	HL_3		
HA	–5.04	–7.40	–9.60	2.20×10^{-3}	1.08×10^{-3}	3.18×10^{-3}	6.46×10^{-3}	2.37
FA	–5.19	–7.77	–10.53	1.83×10^{-3}	1.08×10^{-3}	2.42×10^{-3}	2.71×10^{-2}	0.10

* HL_1, HL_2 and HL_3 represent the carboxyl groups (–COOH), the phenolic groups (Ar–OH) and the amine groups ($–NH_2$) of HA and FA, respectively.

the background electrolyte $NaClO_4$, HA(FA), TNTs and Milli-Q water. The radiotracer $^{152+154}$Eu(III) was used in the batch adsorption experiments. In the experiments, HA/FA was first equilibrated with the TNT suspension for 1 day, and then the Eu(III) solution was added to HA/FA-TNT suspension to start the adsorption of Eu(III) on HA/FA-TNT hybrids. The pH value of the solution was adjusted with negligible amounts of $HClO_4$ or NaOH. The blank experiments indicated that the adsorption of Eu(III) on the tube walls was negligible. The polyethylene tubes were shaken to obtain adsorption equilibrium, and then the solid was separated from the liquid phase by centrifugation at 18000 rpm for 30 min. The $^{152+154}$Eu(III) concentration in the supernatant was analyzed by liquid scintillation counting (Packard 3100 TR/AB Liquid Scintillation analyzer, PerkinElmer) with ULTIMA GOLD AB^{TM} (Packard) Scintillation cocktail. To take into consideration of Eu(III) loss from procedures expect for adsorption (i.e., Eu(III) adsorption on filters and containers), calibration curves were attained separately under otherwise identical conditions as the adsorption process but no adsorbent. Based on the attained calibration curves, the adsorbed mass of Eu(III) was calculated via subtracting the mass in the solution from the mass spiked. All experimental data were the average of triplicate determinations and the relative errors were about 5%.

2.3 Sample preparation for EXAFS analysis

Adsorption experiments for EXAFS analysis were conducted using a 1 L vessel with 0.5 g/L TNTs, 0.01 mol/L $NaClO_4$ and 4.0×10^{-6} (or 2.0×10^{-3}) mol/L Eu(III) under different experimental conditions. Adsorption was performed by adding 30 mL acidified 10^{-3} mol/L $Eu(ClO_4)_3$ stock solution and appropriate 0.1 mol/L NaOH to neutralize the acidity of this Eu(III) solution. The Eu(III) solution was introduced as follows: 10 μL increments of the Eu(III) stock solutions were introduced into the suspension under constant stirring to disperse the small aliquot of Eu(III) solution, and then the base solution was added. Simultaneously, the pH was monitored and kept to the desired value during Eu(III) addition. Periods of a few minutes between the increments were chosen to avoid Eu(III)(aq) exceeding the solubility limit of $Eu(OH)_3$(s), while allowing the completion of Eu(III) addition in reasonable delay [14]. Finally, the samples were recovered by filtering the suspensions and then slightly drying the pastes under vacuum and ambient temperature.

2.4 EXAFS measurements and analysis

Eu(III) L_{III}-edge EXAFS spectra at 6976.9 eV were recorded at room temperature at Shanghai Synchrotron Radiation Facility (SSRF, China) in fluorescence (for Eu(III)(aq) and adsorption samples) and transmission (for $Eu(OH)_3$(s) and Eu_2O_3) modes. For all adsorption samples, an intense adsorption line at 6985 eV (XANES data not shown) dominates the X-ray absorption edge. The position of this line shows that Eu is trivalent in all adsorption samples [13]. The electron beam energy was 3.5 GeV and the mean stored current was 300 mA. A superconductor wiggler with a maximum magnetic field B_0 of 6 T inserted in the straight section of the storage ring was used. The energy of X-ray was detuned by using a fixed-exit double-crystal Si (111) monochromator. Ionization chambers with N_2 atmosphere were used to collect the Eu(III) L_{III}-edge spectra in transmission mode at room temperature. A multi-element pixel high purity Ge solid-state detector was used to collect the fluorescence signal. EXAFS data analysis was performed with the Athnea software. The EXAFS oscillations were isolated from the raw, averaged data by removal of the pre-edge background, approximated by a first-order polynomial. The extracted EXAFS spectra, obtained via spline fitting techniques and normalized using a victoreen function, were Fourier transformed (FT) using the k range of 1.6–10.0 $Å^{-1}$. The curve-fitting analysis was carried out using the IFEFFIT engine-based interface, Six-PACK. The theoretical scattering phases and amplitudes used in data analysis were calculated with the scattering code FEFF7 using the crystal structures of $Eu(OH)_3$, Eu_2O_3 and $Eu_2Ti_2O_7$.

3 Results and discussion

3.1 Characterization of TNTs

Figure 1 shows the FE-SEM and TEM images of TNTs. The tube structures of 10 nm in outer diameter and hundreds nanometers in length are observed. The layer structure of mostly 3-fold can be recognized. No particulate structure of the TiO_2 precursor was found in every view field, indicating that the whole TiO_2 was converted to TNTs by hydrothermal synthesis. ICP-MS analysis showed that the as-prepared TNTs contained Na atoms of ~0.15 wt%. As can be seen from the TEM image, TNTs had well-defined and uniformly tubular morphology. Compared with carbon nanotubes, the TNTs were less adhesive to each other; the tube ends were released and kept open.

The results are quite similar to those reported in the literatures [19, 20].

Figure 2 shows the XRD patterns of the as-prepared

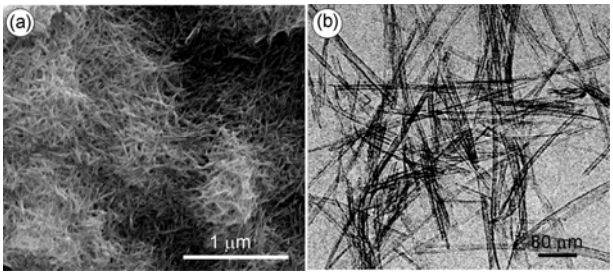

Figure 1 FE-SEM (a) and TEM images (b) of the as-prepared TNTs.

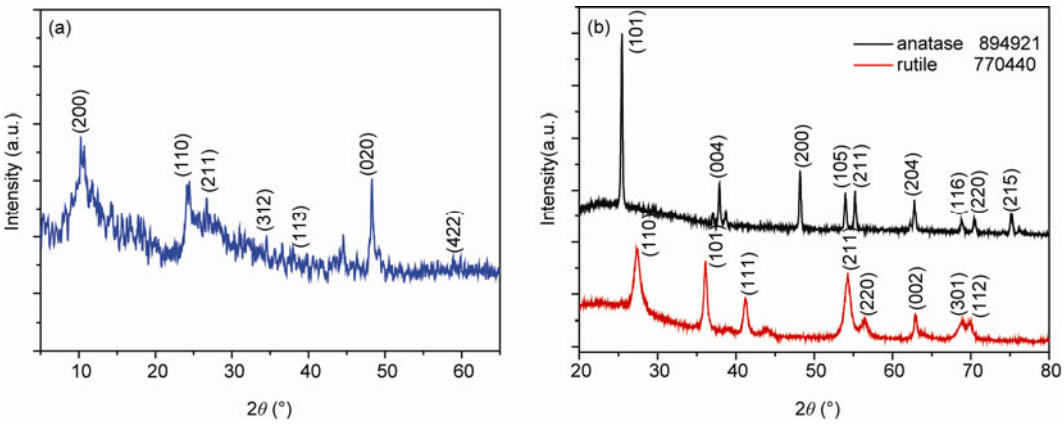

Figure 2 XRD patterns of the as-prepared TNTs (a) and commercial TiO_2 (anatase and rutile) (b).

TNTs and commercial TiO_2 (anatase and rutile). The XRD pattern of the as-prepared TNTs (Figure 2(a)) agrees well with that appears in references [19], where the indices were determined based on the calculation for a scrolled titanate nanosheet ($H_2Ti_3O_7$). All the observed XRD peaks ($2\theta \approx$ 10°, 25°, 29° and 50°) were assigned to TNTs, and the intense peak at about 10° was attributed to interlayer space of TNTs, which was in accordance with the previous report [19]. The XRD patterns indicated that the TiO_2 precursors were completely transformed to TNTs and no anatase or rutile phase appeared in the as-prepared TNTs. These results were in good consistency with the previous study [19]. For comparison, the XRD patterns of commercial TiO_2 (anatase and rutile) were also presented in Figure 2(b).

Figure 3 shows the Fourier transform infrared (FTIR) spectrum of the as-prepared TNT samples. The spectrum of the as-prepared TNTs exhibits a broad and intense band located at about 3200 cm^{-1}, which is attributed to the O–H stretching mode, indicating the presence of surface hydroxyl groups and water molecules adsorbed on the surface and in the interlayer space of the TNTs. Water molecules were confirmed by the presence of the band at 1600 cm^{-1} that is assigned to the H–O–H deformation mode. The band observed at 895 cm^{-1} can be attributed to the Ti–O stretching mode which involves non-bridging oxygen atoms. The band at 490 cm^{-1} is related to Ti–O–Ti vibrations of the interconnected octahedra that are rigid units responsible for the formation of the TNT walls. The observations are in good agreement with the structures of TNTs [7, 21].

The N_2 adsorption-desorption isotherms and corresponding Barrett, Joyner and Halenda (BJH) pore-size distribution curve of the as-prepared TNT samples are shown in Figure 4. The stepwise adsorption and desorption isotherm is indicative of 1D intersection of a solid porous material [22]. The average pore size for the TNT samples is 10.625 nm with a wide distribution of pore size. It is obvious that mecropore is dominant of the total pore volume of the as-prepared TNTs. The specific surface area and monolayer capacity of the as-prepared TNTs are 406.8 m^2/g and 93.5 cm^3/g, respectively. It can be seen that the synthesis process of TNTs derived from commercial TiO_2 (P25) results in an obvious increase in surface area and porosity. This is increased by a factor of 9 compared with that of Degussa P25 (46.9 m^2/g) [4, 6]. With respect to commercial TiO_2 (P25), the high specific surface area and porosity of as-prepared TNTs make it possible to have large sorption ability towards metal ions.

3.2 Macroscopic and EXAFS study of Eu(III) adsorption on TNTs

The k^2-weighted, normalized, background-subtracted EXAFS spectra (a) and radial structure functions (RSFs) (b) produced by forward Fourier transforms (uncorrected for phase shift) for the reference samples (Eu(III)(aq), $Eu(OH)_3$, and Eu_2O_3) are shown in Figure 5. The EXAFS spectrum of the Eu(III)(aq) solution, which shows a single sinusoidal oscillation due to the backscatter of oxygen atoms in the first shell, provides a good example of an outer-sphere complex of Eu(III). The only single peak at about 1.9 Å (phase shift uncorrected) indicates a single shell of backscatter atoms neighboring the central Eu atom. Eu(III)

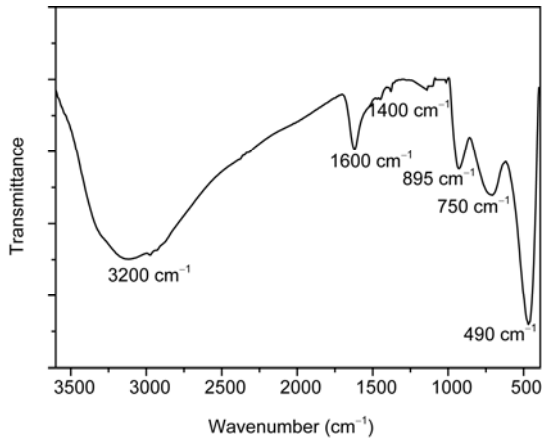

Figure 3 Fourier transform infrared (FTIR) spectrum of the as-prepared TNTs.

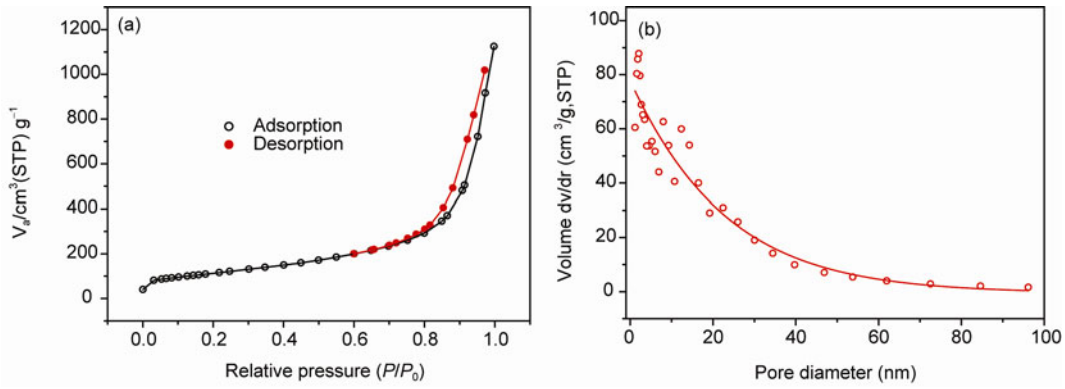

Figure 4 N_2 adsorption-desorption isotherms (a) and corresponding BJH pore-size distribution curve (b) of the as-prepared TNTs. The pore-size distribution was calculated from the desorption branch of the isotherm.

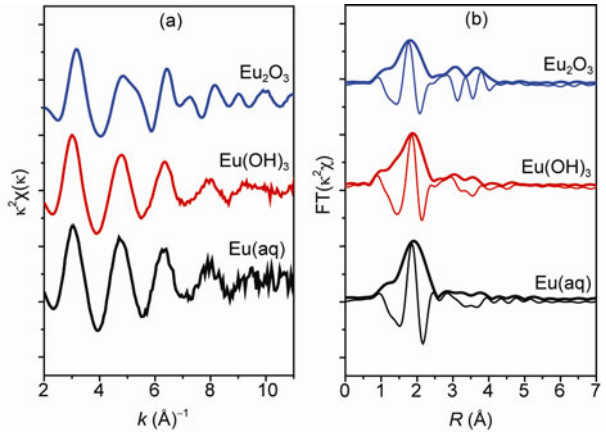

Figure 5 k^2-weighted, normalized, background-subtracted EXAFS spectra (a) and the corresponding FTs magnitudes and imaginary parts of the reference samples (Eu(III)(aq), $Eu(OH)_3$, and Eu_2O_3) (b).

is coordinated with 8.9 oxygen atoms at interatomic bond distance of 2.426 Å in Eu(III)(aq) solution (Table 3). This result is in good agreement with other results of recent EXAFS studies. For example, Schlegel *et al*. [13] found that Eu(III) (aq) solution (at pH 3.6) had a 9-fold coordination of Eu(III) with the Eu–O bond distance of 2.427 Å in the first shell. It has been observed by Tan *et al*. [12] that Eu(III) was coordinated with 8.8 oxygen atoms at interatomic bond distance of 2.427 Å in Eu(III)(aq) solution. Fan *et al*. [11] also reported the Eu–O bond distance of Eu(III)(aq) in acidic solution was 2.418 Å where the coordination number of the oxygen in the first shell was held constant at 9.24. In the R-space fit, a value for N of 8.9, somewhat smaller than 9, is obtained. It appears tempting to interpret the determined 8 < N < 9 as an indication of an equilibrium between octa and nonahydrated species, similar to that for the intermediate lanthanide aquo species between Am(III), Gd(III) and Sm(III) [15].

In contrast to aqueous Eu(III)(aq), $Eu(OH)_3$ and Eu_2O_3 show more complex structural features in the overall k range of χ-function EXAFS spectra. These features indicate the presence of heavy backscatter atoms surrounding Eu in higher shells. Because of the contribution of higher-shell atoms in the coordination environment of Eu(III), the χ-function EXAFS spectra of Eu_2O_3(s) and $Eu(OH)_3$(s) have more distinct structural features than appear for aqueous Eu(III)(aq). Fourier transformed RSFs of these spectra indicate that some of this backscatter was due to the existence of higher shells.

For $Eu(OH)_3$(s), the Eu–O bond distance in the first shell was 2.416 Å with 7.9 oxygen atoms, and the second shell had Eu–Eu bond with interatomic distance of 3.61 Å and coordination numbers of 2.2. For Eu_2O_3(s) coordination environment, in the first shell, the Eu–O bond distance was 2.346 Å with coordination number of 6.2 oxygen atoms. The second shell of Eu_2O_3(s) was fitted only with Eu–Eu contribution with coordination number of 6.4 at Eu–Eu bond distance of 3.59 Å. The EXAFS results of the three reference samples are quite in agreement with the results of the three samples reported in the literatures [11, 12].

3.2.1 *Kinetic study*

Adsorption of Eu(III) on TNTs (Figure 6) was studied at pH

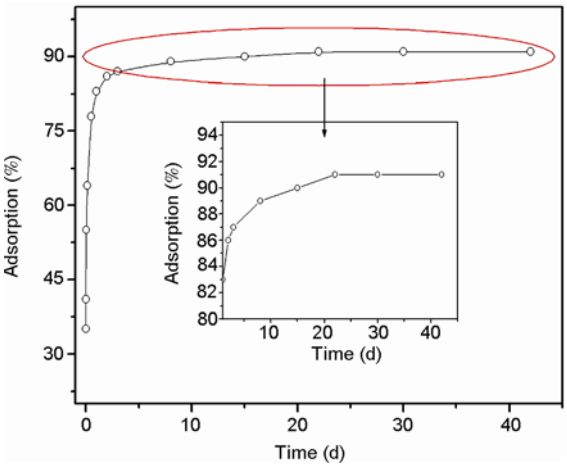

Figure 6 Effect of contact time on Eu(III) adsorption onto TNTs, T = 20 ± 1 °C, $C_{(Eu)initial}$ = 4.0×10^{-6} mol/L, m/V = 0.5 g/L, I = 0.01 mol/L $NaClO_4$, pH 6.0.

Table 3 Structure parameters derived from EXAFS data analysis of reference samples and adsorption samples at Eu L_{III}-edge.

Sample conditions	First shell (Eu–O)			Second shell (Eu–Eu/Ti)				
	N	R (Å)	σ^2 (Å^2)	bond	N	R (Å)	σ^2 (Å^2)	R_f
Eu(aq)	9.1	2.425	0.0085					0.034
$Eu(OH)_3$	7.8	2.416	0.0082	Eu–Eu	2.4	3.63	0.0011	0.008
Eu_2O_3	6.4	2.347	0.0104	Eu–Eu	6.2	3.58	0.0074	0.011
pH 4.0, 30 d, 4.0×10^{-6} M	8.9	2.417	0.0112					0.015
pH 6.0, 30 d, 4.0×10^{-6} M	8.7	2.408	0.0125	Eu–Ti	1.3	4.42	0.0085	0.032
pH 8.0, 30 d, 4.0×10^{-6} M	8.3	2.403	0.0124	Eu–Ti Eu–Eu	1.5 2.2	4.41 3.64	0.0058 0.0061	0.025
pH 10.0, 30 d, 4.0×10^{-6} M	7.5	2.402	0.0165	Eu–Ti Eu–Eu	1.3 2.5	4.42 3.62	0.0076 0.0058	0.023
pH 6.0, 30 d, 2.0×10^{-3} M	8.6	2.414	0.0145	Eu–Ti Eu–Eu	1.2 3.1	4.41 3.62	0.0067 0.0072	0.019
pH 6.0, 2 d, 4.0×10^{-6} M	9.1	2.415	0.0112	Eu–Ti	1.1	4.41	0.0073	0.021
pH 6.0, 60 d, 4.0×10^{-6} M	8.8	2.411	0.0122	Eu–Ti Eu–Eu	1.3 2.7	4.42 3.64	0.0054 0.0055	0.017
pH 6.0, 30 d, 4.0×10^{-6} M, 10 mg/L HA	8.5	2.405	0.0113	Eu–Ti Eu–C	1.2 2.3	4.42 2.72	0.0063 0.0064	0.024
pH 6.0, 30 d, 4.0×10^{-6} M, 10 mg/L FA	8.5	2.405	0.0114	Eu–Ti Eu–C	1.4 2.1	4.41 2.72	0.0063 0.0058	0.044

R, interatomic distance; N, number of neighbor oxygens; σ^2, Debye-Waller factor; R_f , the residual factor; $R_f = \sum_k(k^2x_{exp}-k^2x_{calc})/\sum_k(k^2x_{exp})$ measures the quality of the model Fourier-filtered contribution (x_{calc}) with respect to the experimental contribution (x_{exp}). Eu(aq), $Eu(OH)_3$ and Eu_2O_3 are named as reference samples, whereas the other samples with adsorbed Eu(III) are named as adsorption samples.

6.0 as a function of the contact time for trace metal ion concentrations. The adsorption was shown to be rapid and a contact time of 2 days was enough to reach equilibrium. The adsorption was initially fast in several hours, and slowly in the following contact time.

This two-step adsorption process follows the general behavior of metal adsorption at solid-water interfaces [23]. Several mechanisms have been proposed for the slow continued metal uptake at solid surfaces, including adsorption of metals onto sites that have relatively large activation energies, diffusion into micropores of TNTs, and a continuous growth of a surface precipitate [23–25].

The EXAFS spectra measured at contact time of 2, 30 and 60 days, respectively, are reported in Figure 7(a). The RSFs of the three adsorption samples exhibit a characteristic peak at ~1.9 Å (phase shift uncorrected) due to the O atoms and two higher-shell peaks at ~3.1 Å and ~4.1 Å (phase shift uncorrected) due to the backscatter of Eu or Ti atoms, respectively (Figure 7(b)).

For the adsorption sample of 2 days, the higher shells could be due to Eu or Ti atoms because of only Eu or Ti atoms in TNTs. The first shell can be described with ~ 9 O atoms at R ~2.40 Å, which is consistent with the typical 8-9 fold coordination environment of Eu(III) [12].

The second shell at ~4.1 Å (phase shift uncorrected) is an evidence of the formation of an inner-sphere complex [12]. The fit leads to R_{Eu-Ti} equals to 4.42 Å with a fixed N_{Eu-Ti} of 1 at the second shell (see Table 3). Similar results can be also obtained at 30 days (Table 3 and Figure 7). However, when the contact time increases to 60 days, an additional

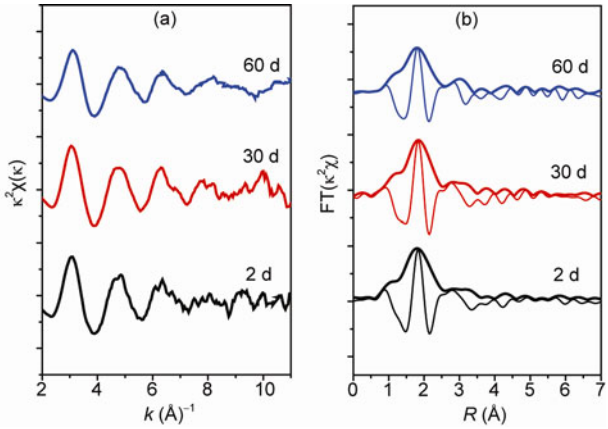

Figure 7 (a) The normalized, background-subtracted and k^2-weighted EXAFS spectra and (b) the corresponding FTs magnitudes and imaginary parts of Eu(III) adsorption samples at various contact time, t = 2, 30, 60 d, m/V = 0.5 g/L, $C_{Eu(III)initial} = 4.0\times10^{-6}$ mol/L, pH 6.0, T = 20 ± 1 °C, I = 0.01 mol/L $NaClO_4$.

peak at ~3.1 Å can be observed. It can be well fitted by R_{Eu-Eu} of 3.62 Å with a fixed N_{Eu-Eu} of 2 Eu atoms. This indicates the formation of multinuclear metal species or surface precipitates at long contact time. The time-variant nature of spectra is similar to earlier report in which continued metal uptake is attributed to the formation of surface-induced metal polymer or precipitation that is accompanied by growth of second-shell metal-metal backscatter features [23]. However, this finding is contradictory with reports of surface or intraparticle diffusion processes, which is responsible for the slow metal uptake mechanism [23, 25]. In

the following, we will limit the contact time to less than 30 days to avoid the formation of surface precipitates or multinuclear metal species.

3.2.2 *pH effect*

The pH effect on Eu(III) adsorption to TNTs is presented in Figure 8(a). A pronounced increase of Eu(III) adsorption from almost zero to ~95% within the pH range of 2.0–6.0 is observed and then the adsorption of Eu(III) remains constant with increasing pH. The LogK_d (distribution coefficient, $K_d = \frac{C_0 - C_e}{C_e} \times \frac{V}{m}$, where C_0 is the initial concentration, C_e is the final concentration of Eu(III) in supernatant, V is the volume and m is the mass of TNTs) values at pH > 6.0 are 5.0 ± 0.6 for different ionic strengths, and no difference is found under the experimental uncertainties. The results are consistent with those of Eu(III) adsorption on hydrous alumina [10], attapulgite [11], natural hematite [26] and carbon nanotube/iron oxide magnetic composites [27].

The adsorption properties of TNTs are strongly dependent on its surface properties. Various functional groups such as ≡TiOHTi≡ (hydroxylated bridging groups), ≡TiOH (terminal uncharged surface groups), $\equiv TiOH_2^+$ (positively charged groups) and $\equiv TiO^-$ (negatively charged groups) are present at the surface of TNTs. With increasing pH, these functional groups are progressively deprotonated, forming negative surface charge. The attractive force between the negative surface sites and positive metal ions results in the formation of metal-ligand TNT complexes [12]. The adsorption at pH < 6.0 is influenced by ionic strength obviously, whereas no drastic difference of Eu(III) adsorption on TNTs is found at pH > 6.0. The effect of ionic strength on the adsorption reaction can be used to evaluate the adsorption mechanism [28]. The background electrolyte concentration influences the thickness and interface potential of the double layer, affecting the binding of the sorbing species. β-plane adsorption can be assumed to occur when ionic strength easily influences the adsorption; otherwise, o-plane adsorption may occur [28]. From the results, one can draw a conclusion that β-plane adsorption and ion exchange or outer-sphere surface complexation contribute to Eu(III) adsorption on TNTs at pH < 6.0, while an o-plane adsorption and/or inner-sphere surface complexation dominate Eu(III) adsorption at pH > 6.0. The results are quite similar to the effect of pH and ionic strength on Eu(III) adsorption to attapulgite [11] and ZSM-5 zeolite [29]. Figure 8(b) shows pH effect at different initial Eu(III) concentrations. The curves show a typical "adsorption edge", namely, the percentage of uptake increases from practically zero to ~95% over a range of more than three pH units. As expected, the pH-edge shifts to higher pH values at higher Eu(III) concentrations, which is consistent with the results of Eu(III) adsorption on natural hematite [26]. Similar results were also observed for Eu(III) adsorption onto attapulgite [11] and carbon nanotube/iron oxide magnetic

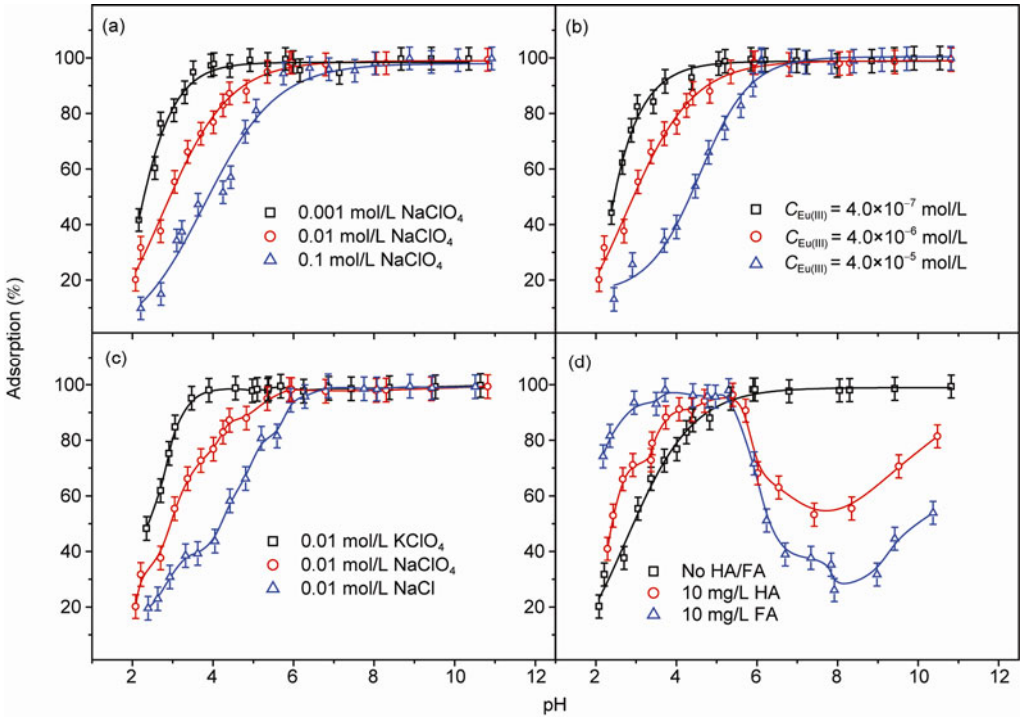

Figure 8 Adsorption of Eu(III) on TNTs as a function of pH, T = 20 ± 1 °C, m/V = 0.5 g/L, contact time = 30 d. (a) Effect of ionic strength, $C_{(Eu)initial}$ = 4.0×10^{-6} mol/L; (b) effect of initial Eu(III) concentrations, I = 0.01 mol/L $NaClO_4$; (c) effect of foreign cations and anions, $C_{(Eu)initial}$ = 4.0×10^{-6} mol/L; (d) effect of HA and FA, $C_{(Eu)initial}$ = 4.0×10^{-6} mol/L, I = 0.01 mol/L $NaClO_4$.

composites [27]. However, in our previous study, it was found that the sorption of Eu(III) on anatase and rutile is strongly dependent on pH values and independent of ionic strength, which indicates the formation of an inner-sphere complex [12].

The pH effect on Eu(III) adsorption to TNTs in 0.01 mol/L $KClO_4$, $NaClO_4$ and NaCl solutions, respectively, is illustrated in Figure 8(c). The cations influence the adsorption of Eu(III) on TNTs drastically at pH < 6.0, suggesting that the cations can change the surface properties of TNTs and thus affects the interaction of Eu(III) with TNTs. Before the addition of Eu(III), K^+/Na^+ has achieved equilibrium on TNT surfaces. Hence, the adsorption of Eu(III) on TNTs can be considered as an exchange of Eu(III) with surface adsorbed K^+/Na^+. The adsorption curve shifts to left in $KClO_4$ solution as compared to that in $NaClO_4$ solution, i.e., the order of adsorption percentage of Eu(III) on TNTs is higher for K^+ than that for Na^+, which might be ascribed to the fact that the hydrated ionic radius of K^+ (2.32 Å) is smaller than that of Na^+ (2.76 Å) [30, 31]. Na^+ has higher affinity to the surface of TNTs and higher tendency for counter-ion exchange with the surface active sites, which reduces Eu(III) adsorption on TNTs. The outer-sphere surface complexes are mainly present in the sorption process because of the surface of TNT possesses large negative charge and specific surface area [32]. This phenomenon could be attributed to two reasons: (1) Eu(III) ions form electrical double layer complexes with TNTs, which favors the sorption when the concentration of the competing salt is decreased. This may indicate that the sorption interaction between the functional groups of TNTs and Eu(III) ions is mainly an ionic interaction, which is in good agreement with the ion exchange mechanism; (2) cations can impact particle aggregation by affecting electrostatic interactions. Increased ionic strength has shown to reduce electrostatic repulsion and thereby increases particle aggregation of TNTs, which reduces the amount of available binding sites and thereby decreases the sorption of Eu(III) on TNTs. However, at pH > 6.0, no drastic difference of Eu(III) adsorption in $NaClO_4$ and $KClO_4$ solutions is observed, which may be attributed to the inner-sphere surface complexation in this pH range. Figure 8(c) also demonstrates that adsorption curve of Eu(III) in NaCl solution is lower than that of Eu(III) in $NaClO_4$ solution at pH < 6.0. This may be attributed to the facts that: (I) Cl^- can form soluble complexes with Eu(III) in solution (e.g. $EuCl_x^{(2-x)-}$), while ClO_4^- does not form soluble complexes with Eu(III) in solution. Eu(III) has high affinity to Cl^- but low affinity to ClO_4^-; (II) idiocratic adsorption of Cl^- to TNTs is a little easier than that of ClO_4^-, and Cl^- adsorption on the surface of TNTs changes the surface properties of TNTs and decreases the availability of binding sites for Eu(III); (III) the smaller radius inorganic acid radicals of Cl^- can take up more ion exchange sites and therefore lead to the decline of Eu(III) adsorption on TNTs. To understand the adsorption mechanism, the initial and final of pH were also measured. The equilibrium pH values are plotted as a function of initial pH values for each experimental data is shown in Figure 9.

The dotted line represents that the pH values do not

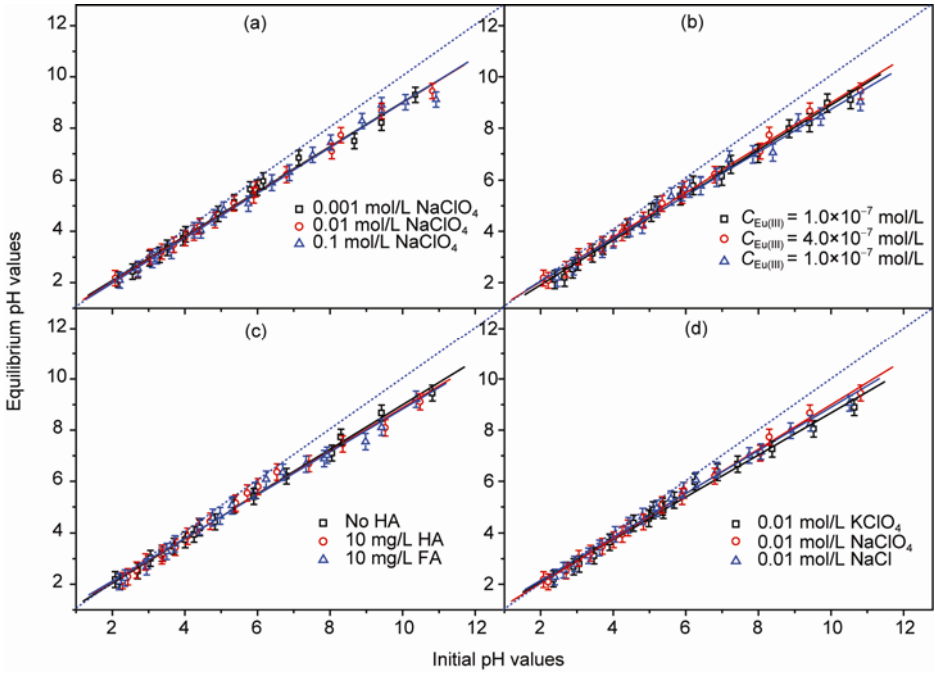

Figure 9 Equilibrium pH values vs. initial pH values of Eu(III) adsorption onto TNTs, T = 20 ± 1 °C, m/V = 0.5 g/L. (a) $C_{(Eu)initial}$ = 4.0×10^{-6} mol/L, at different $NaClO_4$ concentrations; (b) I = 0.01 mol/L $NaClO_4$, at different initial Eu(III) concentrations; (c) $C_{(Eu)initial}$ = 4.0×10^{-6} mol/L, in the presence or absence of HA/FA; (d) $C_{(Eu)initial}$ = 4.0×10^{-6} mol/L, in the presence of different cations and anions.

change during the adsorption process. However, it can be obviously seen that the equilibrium pH values are lower than the initial ones with a value which increases with increasing of the initial pH in the whole pH range. The relationship between the initial and equilibrium pH values is almost linear. The exchange reaction of Eu(III) ions with the hydroxyls on the surface of TNTs is presumed as the following equation: $TiOH^{3+} + Eu^{3+} = TiOEu^{5+} + H^+$. Since the hydrogen ion concentration increased with an increasing adsorption amount of Eu(III) ions on TNT surfaces, the pH value changed to the acidic region as shown in Figure 9.

The EXAFS spectrum of the adsorption sample obtained at pH 4.0 (Figure 10) is close to that of Eu(III)(aq) (Figure 5). Only a single broad peak at ~1.9 Å is observed in the RSF. This peak is resulted from O backscatter in the first coordination shell of Eu atom. The large width of this peak indicates a high degree of disorder. The spectral noise is pronounced due to low amount of Eu(III) adsorbed on TNTs at this low pH. This is a result of dampening of the EXAFS signal due to large amount of structural and thermal disorder, and the lack of heavy backscatter atoms in the local atomic structures [33]. This indicates that the local atomic structure of adsorbed Eu(III) is similar to that of Eu(III)(aq) and an outer-sphere surface complex is formed at this low pH. This is coherent with macroscopic data. An outer-sphere surface complex is adsorbed to the surface via electrostatic interaction and is sensitive to ionic strength and medium composition [28]. This is illustrated in Figure 10(a), i.e., the more the ionic strength, the less the interaction.

The EXAFS spectra of the adsorption samples obtained at pH 6.0, 8.0 and 10.0 are quite different from that obtained at pH 4.0 (Figure 10). All the EXAFS spectra of the adsorption samples have multi frequency wave shape. These features indicate the presence of more than one ordered neighboring shells around Eu atom. Outer-sphere surface complex is not the main adsorption mode for these adsorption

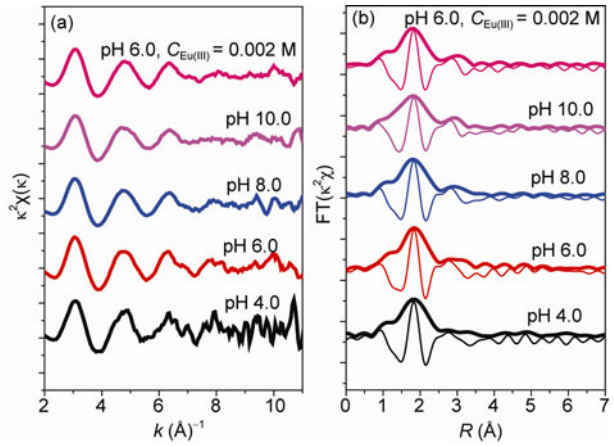

Figure 10 (a) The normalized, background-subtracted and k^2-weighted EXAFS spectra and (b) the corresponding FTs magnitudes and imaginary parts of Eu(III) adsorption samples at various pH values and initial Eu(III) concentrations, m/V = 0.5 g/L, $C_{Eu(III)initial}$ = 4.0×10^{-6} or 2.0×10^{-3} mol/L, pH = 4.0, 6.0, 8.0 and 10.0, T = 20 ± 1 °C, I = 0.01 mol/L $NaClO_4$.

samples. The mode at k ~6 Å^{-1} gradually increases in intensity with increasing pH, and the spectral feature between 7 to 9 Å^{-1} seemingly evolves, although this evolution is partly obscured by the spectral noise at low Eu(III) loading. These two spectral modifications indicate a change of Eu(III) coordination structures over pH.

As indicated in the previous section, the second shell at ~4.1 Å (phase shift uncorrected) corresponding to Eu–Ti backscatter is an evidence of the formation of an inner-sphere complexation [34]. This is further illustrated by the change in the bond distance of Eu–O; it is shorter at pH 6.0 (R_{Eu-O} = 2.408 Å) than pH 4.0 (R_{Eu-O} = 2.417 Å). This is a direct indication of the interaction of Eu with both O from water and O from the surface. The length of Eu–OH bond is expected to be shorter than Eu–O bond associated with those of coordinated water molecules and the oxygen atoms of surface binding sites. However, it is not possible to distinguish the two shells by fitting since the difference in bond distance is not enough obvious. This is in agreement with macroscopic data, an o-plane adsorption dominates Eu(III) adsorption mechanism [21].

When the pH continues to increase, similar spectra were also obtained with a few differences. First, there is a decrease in N_{Eu-O}. It may not necessarily result from an actual decrease in the overall coordination number but rather result from the introduction of more asymmetry in the Eu–O coordination sphere. A loss in EXAFS oscillatory intensity can be caused by destructive interferences of a number of oscillations having small differences in their frequencies, due to a variation in their interatomic distances. Secondly, an additional shell appears at 3.10 Å with continues increasing pH. The small peak at ~4.1 Å is suggestive of Ti backscatter and also indicates the formation of inner-sphere surface complexes. For the adsorption sample at pH 10.0, the backscatter from O atom in the first shell is dominated by a peak with a center at ~1.8 Å, indicating the R_{Eu-O} value is shorter than the R_{Eu-O} value for other samples (peak at ~1.9 Å) [33]. The fit for this shell indicates that the presence of Eu atom at an average R_{Eu-Eu} value of 3.60 Å with a fixed N_{Eu-Eu} value of ~2 Eu atoms, which is suggestive of the formation of some surface or even polynuclear Eu complexes at the surface of TNTs. Such a result was as also well observed at pH 6.0 for t = 60 days (see previous section) or when Eu concentration increases to 2.0×10^{-3} mol/L (Figure 10 and Table 3).

For the adsorption samples obtained at pH 6.0, the fit for the high shell indicates the presence of a high neighbor Ti atom at R_{Eu-Ti} of 4.41–4.42 Å and N_{Eu-Ti} of ~1 Ti atom for $C_{Eu(III)}$ = 4.0×10^{-6} M, whereas the presence of Eu atom at R_{Eu-Ti} of 4.41 Å and N_{Eu-Ti} of ~1 Ti atom and R_{Eu-Eu} of 3.62 Å with a fixed N_{Eu-Eu} of ~3 Eu atoms for $C_{Eu(III)}$ = 2.0×10^{-3} M. The observed results support the formation of inner-sphere surface complexes and/or some polynuclear Eu complexes at the surface of TNTs. Bouby *et al*. [34] studied the sorption of Eu(III) on commercially available TiO_2

(Degussa P-25) as a function of pH and ionic strength by a combination of macroscopic and EXAFS technique. The macroscopic sorption results showed that the sorption of Eu(III) was independent of ionic strength. EXAFS spectroscopic was conducted in a narrow pH range (i.e., pH 6.3–7.2) and the results indicated the formation of inner-sphere surface complexation, and the sorption mechanism, local atomic structures and species were invariant with pH ranging from 6.3 to 7.2. Herein, the sorption of Eu(III) on TNTs as a function of pH and ionic strength was investigated by a combination of macroscopic and EXAFS technique in a wide pH range (i.e., pH 4.0–10.0). It was interesting to find that the sorption mechanism, local atomic structures and species were variant with pH changing, i.e., outer-sphere surface complexation dominated Eu(III) sorption at pH 4.0, whereas inner-sphere surface complexation was the main sorption mechanism at pH 6.0–8.0. At pH 10.0, Eu polynuclear complexes and surface precipitates began to form at the surface of TNTs. At pH 6.0–8.0, the results of this paper were in good agreement with those reported by Bouby *et al*. [34]. However, Bouby *et al*. [34] did not investigate the mechanism and local atomic structures of Eu(III) sorption on TiO_2 at low and high pH values.

3.2.3 HA/FA effect

The adsorption of Eu(III) on TNTs in the presence or absence of HA or FA as a function of pH is shown in Figure 8D. The presence of HA/FA has a significant effect on Eu(III) adsorption to TNTs. Comparing to Eu(III) adsorption on bare TNTs, a sharp increase of adsorption at pH < 6.0 is observed in the presence of HA/FA. This could be due to: (1) the enhancement of Eu(III) adsorption is expected owing to the complexation of Eu(III) with surface adsorbed HA/FA; (2) surface adsorbed HA/FA produces a more negative charge which results in the more electrostatic favorable Eu(III) adsorption. The adsorption of HA/FA on TNTs as a function of pH is shown in Figure 11. With increasing pH values, the adsorption of HA/FA on TNTs decreases due to both electrostatic effects and surface complexation reactions [35]. The samples of HA and FA were extracted from the same soil sample and both of them are chemically heterogeneous compounds containing similar functional groups at different proportions and configurations, such as carboxyl groups, amine groups and phenolic groups, and these functional groups play an important role in affecting HA and FA adsorption on TNTs. These similar structural properties indicates the similarity of adsorption property of HA and FA on TNTs.

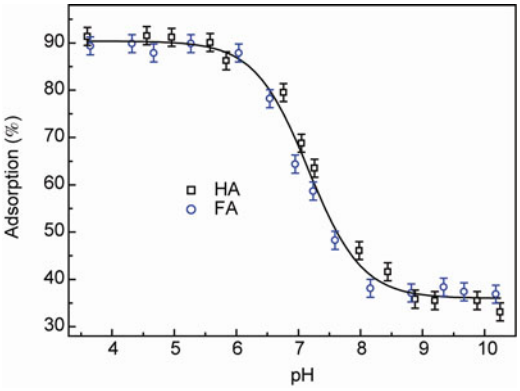

Figure 11 Adsorption of HA and FA on TNTs as a function of pH, $C_{(HA/FA)}$ = 10.0 mg/L, TNT content = 0.5 g/L, I = 0.01 mol/L $NaClO_4$, T = 20 ± 1 °C.

At intermediate pH, adsorption of Eu(III) on HA/FA-TNT hybrids is consistently lower than that of Eu(III) on bare TNTs. The mechanism of Eu(III) adsorption is overlaying by the aqueous Eu(III) species and the formation of $Eu(CO_3)^+$(HA/FA) and $Eu(OH)^{2+}$(HA) in solution [35, 36]. The aqueous Eu(III) species in combination with the increased free HA/FA in solution lead to a lower amount of Eu(III) adsorbed on TNTs. At pH > 8.0, the adsorption rises again slightly, which is due to the following factor: The low level of HA/FA adsorption, coupled with the very large surface area on the colloids, provides evidence of Eu(III) adsorption which is similar to the adsorption of Eu(III) on bare TNTs. However, the adsorption does not reach the levels achieved in the systems free of HA/FA because of either residual soluble $Eu(CO_3)^+$(HA/FA) complexes remained in solution or residual HA/FA on solid surface enhancing electrostatic repulsion between $Eu(CO_3)_2^-$ and TNT surface [37, 38].

It is very interesting to find that the influence of FA on Eu(III) adsorption is a little stronger than that of HA in the whole pH range at the same mass concentrations of HA and FA. HA and FA are chemically heterogeneous compounds containing different types of functional groups at different proportions and configurations. HA and FA contain carboxyl groups, amine groups and phenolic groups [10], and these functional groups play an important role in affecting Eu(III) adsorption on TNTs. Although the samples of HA and FA were extracted from the same soil sample and both of them contain similar functional groups, the proportions and configurations of these functional groups and surface site densities are different. The quantitative concentrations of functional groups of HA and FA are illustrated in Table 2, the surface site density of FA (i.e., 2.71×10^{-2} mol/g) is higher than that of HA (i.e., 6.46×10^{-3} mol/g), which can provide more available surface sites for binding Eu(III). Furthermore, the functional groups of FA such as –OH and –COOH would be ionized as pH increased, leading to the disappearing of these hydrogen-bond donors of FA and the increase of FA solubility (i.e., the decrease of hydrophobic effects) [36]. Therefore, it is reasonable that FA has a stronger effect on Eu(III) adsorption than HA in the whole pH range.

In the presence of HA or FA, Eu(III) ions are adsorbed by forming a mixture of surface complexes, some containing Eu(III)-surface hydroxyl bonds (i.e., binary Eu(III)-TNTs and type A metal-bridging ternary surface complexes)

and some lacking direct Eu(III)-surface hydroxyl bonding (i.e., type B ligand-bridging ternary surface complexes), and the relative contribution of the individual complexes varies with solution chemistry. Sorption trends agree with earlier reports of metal sorption in metal oxide suspensions containing humic substances [25]. Addition of HA or FA increases Eu(III) sorption at low pH and decreases sorption at high pH. Enhanced metal sorption at low pH, where humic sorption is high, has been attributed to the formation of type B ternary surface complexes where the metal ion is complexed by humic molecules that are simultaneously adsorbed to the mineral surface [24, 25]. Alternatively, humic-promoted metal sorption is sometimes attributed to a reduction in the net positive surface charge caused by the sorption of negatively charged humic molecules, which contributes to more favorable electrostatic interactions with dissolved metal ions (i.e., lowers the pH_{znpc} of TNTs). Reductions in metal sorption at high pH are generally attributed to the formation of dissolved metal-humic complexes that compete with sorption processes [25].

The k^2-weighted, normalized and background-subtracted $k^2\chi(k)$ function EXAFS spectra and the Fourier transformed RSFs of Eu(III) adsorption samples in the presence/absence of HA/FA at pH 6.0, which is indicative of natural environment, are shown in Figure 12. The shell of Eu(III) adsorption on (HA/FA)–TNT hybrids at 6.0 Å decreases markedly in comparison to (HA/FA)-free TNT samples, appearing similar to aqueous Eu-(HA/FA) complexes [11] and suggesting that Eu(III) may be complexed by adsorbed HA/FA on TNT surfaces instead of directly to the TNT surfaces. EXAFS spectra are consistent with the predominance of ligand-bridging Eu(III)–HA(FA)–TNTs ternary complexes. A contribution from Eu–HA–TiO_2 system is observed around 2.7 Å, caused by Eu···C single backscattering and Eu–O–C backscattering [12]. This is attributed to the expected Eu-HA(FA) complexes on the TNT surfaces. The number of carboxylate and phenolate groups bound to Eu could not be determined accurately. However, the spectra show a relatively large contribution from the Eu···C and Eu–O–C backscattering paths at ~2.7 Å. This indicates that the number of bound carboxylate or phenolate groups can be expected to be in the sorption samples, i.e., the substantial complex formation has already taken place after mixing. Complementary spectroscopic experiments reported herein demonstrate that Eu(III) forms binary and ternary inner-sphere complexes with TNTs in the presence of natural organic constituents.

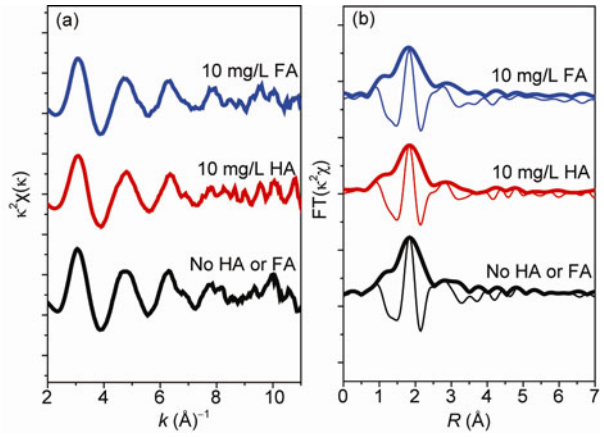

Figure 12 (a) The normalized, background-subtracted and k^2-weighted EXAFS spectra and (b) the corresponding FTs magnitudes and imaginary parts of Eu(III) adsorption samples in the absence or presence of HA/FA, m/V = 0.5 g/L, $C_{Eu(III)initial}$ = 4.0×10^{-6} mol/L, pH 6.0, T = 20 ± 1 °C, I = 0.01 mol/L $NaClO_4$, $C_{(HA/FA)}$ = 10.0 mg/L.

3.2.4 *Adsorption mechanism*

The macroscopic and microscopic results show that Eu(III) could be retained on TNTs via different mechanisms (Figure 13), depending on various environmental conditions such as reaction time, pH and HA/FA. At low pH (i.e., pH 4.0), the uptake of Eu(III) is via outer-sphere surface complexation in the interlayer space (Figure 13I). At pH 6.0 and 8.0, the extent of Eu(III) uptake is increased relative to that at pH 4.0 and is consistent with inner-sphere surface complexation at deprotonated edge sites (Figure 13II). The uptake of Eu(III) at pH 10.0 is attributed to the multinuclear surface complexation (Figure 13III). Adsorbed Eu(III) on HA/FA–TNT hybrids forms both ligand-bridging ternary surface complexes (Eu–HA/FA–TNTs) as well as surface complexes in which Eu(III) remains directly bound to surface hydroxyl groups (i.e., binary Eu–TNTs) of TNTs (Figure 13IV). The attachment of Eu(III) specifically bond to TNT surfaces can reduce their bioavailability and mobility in environmental mediums. The information presented herein will allow scientists and engineers to develop better models that predict the interaction of Eu(III) with TNTs. This study also demonstrates the utility of XAFS to distinguish between different adsorption mechanisms on solid surfaces when they are occurring simultaneously. The findings are important toward a molecular-level description of Eu(III) uptake processes at the water-mineral interface.

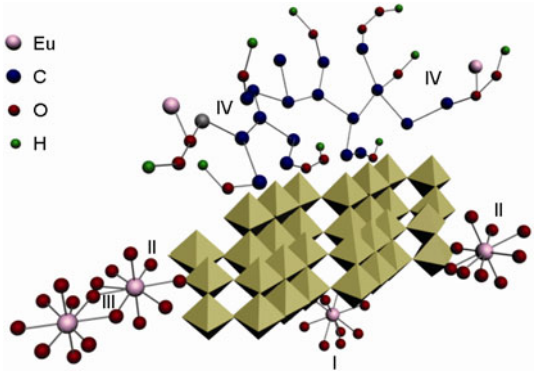

Figure 13 Illustration of possible adsorption sites of Eu(III) on TNTs. I is an example of outer-sphere surface complexation; II is an example of inner-sphere surface complexation, III is multinuclear surface complexation, IV represents the complexation of Eu(III) with surface adsorbed humic substances on TNT surfaces.

4 Conclusions

The complementary results from batch and EXAFS spectroscopy measurements support Eu(III) adsorption by the formation of outer-sphere surface complexes, binary and ternary inner-sphere surface complexes at the TNT-water interface, depending on the solution chemistry. EXAFS spectroscopy analysis indicate that only a single shell from O backscatter exists for adsorbed Eu(III) at pH 4.0, which is in agreement with the formation of outer-sphere surface complexes at the TNT surfaces. While at high pH, the presence of Eu or Ti atoms in the second atomic shell suggests the formation of inner-sphere surface complexes and/or surface polymers on the TNT surfaces. HA/FA may act as a "bridge" between Eu(III) and TNTs. Knowledge obtained from the results will be useful to elucidate the adsorption feature of radionuclides on TNTs. The findings in this study are an important step toward molecular-level description of Eu(III) interaction with nanomaterials and will help to improve our understanding on Eu(III) adsorption processes at the water-solid interface in the natural environment. Despite of their high unit cost at the present time, with the costs of commercially available TNTs decreasing continuously, it is possible to use TNTs for environmental pollutant management in wastewater treatment in near future.

This work was financially supported by the National Natural Science Foundation of China (20907055, 20971126 & 21077107) and the National Basic Research Program of China (2007CB936602 & 2011CB933700). The authors gratefully acknowledge Prof. Yuying Huang and Dr. Xing Gao (SSRF, China) for helpful technical assistance of EXAFS experiments. We also thank Dr. G. Montavon (Subatech, France) for very favorable discussion and comments to improve the quality of the manuscript.

1 Kasuga T, Hiramatsu M, Hoson A, Sekino T, Niihara K. Formation of titanium oxide nanotube. *Langmuir*, 1998, 14: 3160–3163
2 Kasuga T, Hiramatsu M, Hoson A, Sekino T, Niihara K. Titania nanotubes prepared by chemical processing. *Adv Mater*, 1999, 11: 1307–1311
3 Ou HH, Lo SL. Review of titania nanotubes synthesized via the hydrothermal treatment: Fabrication, modification, and application. *Sep Purif Technol*, 2007, 58: 179–191
4 Lee CK, Lin KS, Wu CF, Lyu MD, Lo CC. Effects of synthesis temperature on the microstructures and basic dyes adsorption of titanate nanotubes. *J Hazard Mater*, 2008, 150: 494–503
5 Lee CK, Wang CC, Juang LC, Lyu MD, Hung SH, Liu SS. Effects of sodium content on the microstructures and basic dye cation exchange of titanate nanotubes. *Colloids Surf A*, 2008, 317: 164–173
6 Xiong L, Yang Y, Mai JX, Sun WL, Zhang CY, Wei DP, Chen Q, Ni JR. Adsorption behavior of methylene blue onto titanate nanotubes. *Chem Eng J*, 2010, 156: 313–320
7 Chen YC, Lo SL, Kuo J. Pb(II) adsorption capacity and behavior of titanate nanotubes made by microwave hydrothermal method. *Colloids Surf A*, 2010, 361: 126–131
8 An HQ, Zhu BL, Wu HY, Zhang M, Wang SR, Zhang SM, Wu SH, Huang WP. Synthesis and characterization of titanate and CS_2-modified titanate nanotubes as well as their adsorption capacities for heavy metal ions. *Chem J Chinese U*, 2008, 29: 439–444
9 Liu SS, Lee CK, Chen HC, Wang CC, Juang LC. Application of titanate nanotubes for Cu(II) ions adsorptive removal from aqueous solution. *Chem Eng J*, 2009, 147: 188–193
10 Tan XL, Wang XK, Geckeis H, Rabung Th. Sorption of Eu(III) on humic acid or fulvic acid bound to hydrous alumina studied by SEM-EDS, XPS, TRLFS and batch techniques. *Environ Sci Technol*, 2008, 42: 6532–6537
11 Fan QH, Tan XL, Li JX, Wang XK, Wu WS, Montavon G. Sorption of Eu(III) on attapulgite studied by batch, XPS, and EXAFS techniques. *Environ Sci Technol*, 2009, 43: 5776–5782
12 Tan XL, Fan QH, Wang XK, Grambow B. Eu(III) sorption to TiO_2 (anatase and rutile): Batch, XPS, and EXAFS studies. *Environ Sci Technol*, 2009, 43: 3115–3121
13 Schlegel ML, Pointeau I, Coreau N, Reiller P. Mechanism of europium retention by calcium silicate hydrates: an EXAFS study. *Environ Sci Technol*, 2004, 38: 4423–4431
14 Montavon G, Markai S, Andrés Y, Grambow B. Complexation studies of Eu(III) with alumina-bound polymaleic acid: Effect of organic polymer loading and metal ion concentration. *Environ Sci Technol*, 2002, 36: 3303–3309
15 Stumpf Th, Hennig C, Bauer A, Denecke MA, Fanghänel Th. An EXAFS and TRLFS study of the sorption of trivalent actinides onto smectite and kaolinite. *Radiochim Acta*, 2004, 92: 133–138
16 Tao ZY, Zhang J, Zhai J. Characterization and differentiation of humic acids and fulvic acids in soils from various regions of China by nuclear magnetic resonance spectroscopy. *Anal Chim Acta*, 1999, 395: 199–203
17 Zhang J, Zhai J, Zhao FZ, Tao ZY. Study of soil humic substances by cross-polarization magic angle spinning ^{13}C nuclear magnetic resonance and pyrolysis-capillary gas chromatography. *Anal Chim Acta*, 1999, 378: 177–182
18 Chin YP, Alken G, O'Loughlin E. Molecular weight, polydispersity, and spectroscopic properties of aquatic humic substances. *Environ Sci Technol*, 1994, 28: 1853–1858
19 Suetake J, Nosaka AY, Hodouchi K, Matsubara H, Nosaka Y. Characteristics of titanate nanotube and the states of the confined sodium ions. *J Phys Chem C*, 2008, 112: 18474–18482
20 Niu HY, Wang JM, Shi YL, Cai YQ, Wei FS. Adsorption behavior of arsenic onto protonated titanate nanotubes prepared via hydrothermal method. *Micro Macro Mater*, 2009, 122: 28–35
21 Rodrigues CM, Ferreira OP, Alves OL. Interaction of sodium titanate nanotubes with organic acids and base: Chemical, structural and morphological stabilities. *J Braz Chem Soc*, 2010, 21: 1–8
22 Lee B, Lu D, Kondo JN, Domen K. Three-dimensionally ordered mesoporous niobium oxide. *J Am Chem Soc*, 2002, 124: 11256–11257
23 Lee S, Anderson PR, Bunker GB, Karanfil C. EXAFS study of Zn sorption mechanisms on montmorillonite. *Environ Sci Technol*, 2004, 38: 5426–5432
24 Nachtegaal M, Sparks DL. Nickel sequestration in a kaolinite-humic acid complex. *Environ Sci Technol*, 2003, 37: 529–534
25 Strathmann TJ, Myneni SB. Effect of soil fulvic acid on Nickel(II) sorption and bonding at the aqueous-boehmite (γ-AlOOH) interface. *Environ Sci Technol*, 2005, 39: 4027–4034
26 Rabung Th, Geckeis H, Kim J, Beck HP. The influence of anionic ligands on the sorption behavior of Eu(III) on natural hematite. *Radiochim Acta*, 1998, 82: 243–248
27 Chen CL, Wang XK, Nagatsu M. Europium adsorption on multiwall carbon nanotube/iron oxide magnetic composite in the presence of polyacrylic acid. *Environ Sci Technol*, 2009, 43: 2362–2367
28 Hayes KF, Leckie JO. Modeling ionic strength effects on cation adsorption at hydrous oxide/solution interfaces. *J Colloid Interf Sci*, 1987, 115: 564–572
29 Shao DD, Fan QH, Li JX, Niu ZW, Wu WS, Chen YX, Wang XK. Removal of Eu(III) from aqueous solution using ZSM-5 zeolite. *Micro Macro Mater*, 2009, 123: 1–9
30 Esmadi F, Simm, J. Adsorption of cobalt(II) by amorphous ferric hydroxide. *Colloids Surf A*, 1995, 104, 265–270
31 Shao D, Xu D, Wang S, Fan Q, Wu W, Dong Y, Wang X. Modeling of radionickel sorption on MX-80 bentonite as a function of pH and ionic strength. *Sci China Ser B-Chem*, 2009, 52: 362–371

32 Takamatsu R, Asakura K, Chun W, Miyazaki T, Nakano M. EXAFS studies about the sorption of cadmium ions on montmorillonite. *Chem Lett*, 2006, 35, 224–225
33 Strawn DG, Sparks DL. The use of XAFS to distinguish between inner- and outer-sphere lead adsorption complexes on montmorillonite. *J Colloid Interf Sci*, 1999, 216: 257–269
34 Bouby M, Lützenkirchen J, Dardenne K, Preocanin T, Denecke MA, Klenze R, Geckeis H. Sorption of Eu(III) onto titanium dioxide: Measurements and modeling. *J Colloid Interf Sci*, 2010, 350: 551–561
35 Fairhurst AJ, Warwick P, Richardson S. The influence of humic acid on the sorption of europium onto inorganic colloids as a function of pH. *Colloid Surf A*, 1995, 99: 187–199
36 Geckeis H, Rabung Th, Ngo MT, Kim JI, Beck HP. Humic colloid-borne natural polyvalent metal ions: dissociation experiment. *Environ Sci Technol*, 2002, 36: 2946–2952
37 Yang K, Xing BS. Adsorption of fulvic acid by carbon nanotubes from water. *Environ Pollut*, 2009, 157: 1095–1100
38 Hu J, Xie Z, He B, Sheng G, Chen C, Li J, Chen Y, Wang X. Sorption of Eu(III) on GMZ bentonite in the absence/presence of humic acid studied by batch and XAFS techniques. *Sci China Chem*, 2010, 53: 1420–1428